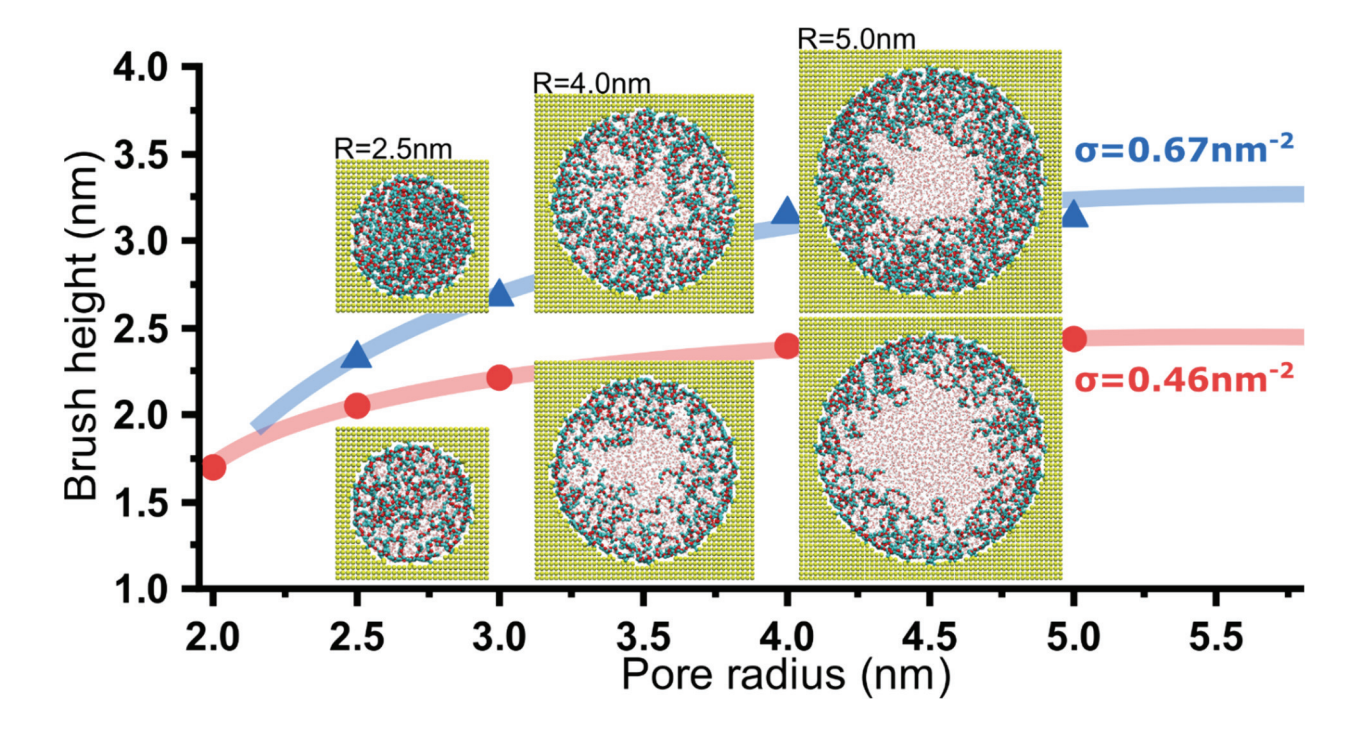
PEO-Grafted Gold Nanopore: Grafting Density, Chain Length and Curvature Effects

Guang Chen† and Elena Dormidontova*,†,‡

†Polymer Program, Institute of Materials Science, University of Connecticut, Storrs, US, 06269 ‡Department of Physics, University of Connecticut, Storrs, US, 06269

E-mail: elena@uconn.edu

For Table of Contents use only:



Abstract

Polymer-grafted nanopores are used in several nanotechnological applications which demand control of structural and hydration properties of the grafted polymers. By means of atomistic molecular dynamics simulations, we systematically investigate the chain length and grafting density effects on the conformation and hydration of polyethylene oxide (PEO) grafted to gold nanopores of different radii. We find that if the pore size exceeds the polymer length, increasing grafting density or chain length for a given pore results in conformational changes of the polymer from pancake-like shapes to well-hydrated overlapping mushrooms to a denser less hydrated polymer brush. We demonstrate that an increase of pore curvature results in considerable polymer crowding within the pore, which translates into an increase of the effective grafting density, $\sigma_{\rm eff}$ which has to be taken into consideration when concave nanopores, planar and convex surfaces are compared. We show that for a given polymer grafting density and chain length a decrease in the pore radius R results in an increased radial orientation and for a low grafting density in a slight increase of grafted layer height H until polymer chains fill the pore (R~H) and start folding near the pore surface, conforming into a cone-shape with a further brush height decrease until the high-density limit is reached. The properties of polymer-grafted nanopores such as water exchange and gating capability depend on the polymer conformation and hydration, which are strongly influenced by the polymer grafting density and differ for polymer-filled and open nanopores.

INTRODUCTION

Polymer-grafted nanopores find an increasing range of nanotechnological applications including membranes for selective ion/nanofluidic transport^{1–4}, DNA translocation⁵, and

gated control.^{6,7} These applications require full control of chain morphology in grafted polymer layers to enable an environment-specific gating capability and/or molecular recognition. To this end understanding the structural properties of polymers grafted within the nanopores, including molecular-level detail, is desirable. While significant progress has been achieved in understanding the general effects of polymer length, grafting density and nanopore size via theoretical,⁸⁻¹⁴ experimental^{1,15,16} and computer modeling research,^{11,17-22} no systematic study at the atomistic level has been attempted so far. In this paper we investigate by means of atomistic molecular dynamics (MD) simulations cylindrical gold nanopores grafted by polyethylene oxide (PEO) chains to understand the interplay of grafting density, chain length and especially nanopore curvature on the structural properties of grafted polymer layers and provide molecular level details on chain conformation and hydration within the nanopores.

PEO has been widely and routinely used for grafting surfaces, including nanopores^{6,15} due to its superior water solubility, biocompatibility²³ and protein adsorption inhibition^{24,25} in biomedical applications. For example, Lim and Deng⁶ grafted a gold nanoring by poly(ethylene glycol) (PEG) for gated control by using 2-propanol as co-solvent exploiting PEG collapse to open the pore. Further, Emilsson *et. al.*¹⁵ studied PEG (of molecular weights 2, 10 and 20 kg/mol) grafted gold coated nanocaves of different diameter to examine the chain length and curvature effect by atomic force microscopy and fluorescent microscopy. They found that longer chains provide a higher coverage of the pore, with a homogeneous monomer density in the radial direction. In addition, they reported an increase and saturation of brush height relative to the pore radius respectively when using PEG with a molecular weight of 10 kg/mol at a grafting density of 0.68 nm⁻² and 20 kg/mol at a grafting

density of 0.28 nm⁻². Thus, there is an evident influence of chain length and grafting density on properties of grafted layers. Furthermore, experimental results for different nanopore systems indicate that pore curvature effect can also be significant. For example, Bayat *et. al.*¹⁶ reported increased polymerization rates and pore filling of anodic aluminum oxide nanopores with high pore curvatures when grafted by poly(diethylene glycol methylether methacrylate), while for very large pore sizes the polymerization kinetics resemble that of flat surfaces. Another study revealed that nanoconfinement effect can significantly affect conductivity and chain conformation of polyelectrolyte brushes grafted to nanopores.²⁶

Previous theoretical considerations and computer simulations provide a solid background for understanding the behavior of polymer-grafted nanopores. 9-16,22,26 For example, coarse-grained (CG) simulations have been applied to study the structural properties of polymers grafted inside a cylindrical nanopore, 11,12,19,27 as well as to investigate the effect of solvent quality on the structural properties of grafted layers. 13,17,20 Different regimes of polymer conformational behavior (mushroom, cigar, brush) have been investigated by CG simulations as functions of chain length and grafting density. It was found that grafted short polymers reside in the vicinity of the surface, while for longer chains the volume fraction distribution is broader, decaying away from the surface and forming a plateau for longer polymers. With an increase of grafting density the polymer volume fraction and layer height increases following a linear dependence on the polymer chain length and approaches the limit of a planar polymer brush for larger pores. Self-consistent field theory and mean field theory^{11,13,14} predict that the brush height of grafted polymer layer scales as $N\sigma^{1/3}$ for moderate and long chain lengths, similar to a planar brush. At the same time the brush height changes non-monotonically with respect to the pore size and can

deviate from $N\sigma^{1/3}$ scaling for nanopores of large curvature. Indeed, a Monte Carlo study of CG polymers grafted to nanopores²² found that the brush height H follows $N^{0.84}\sigma^{0.26}$ dependence within statistical errors. Theoretically, at high pore curvature (small pore sizes), the thickness of grafted polymer layer should be limited by the pore radius R (H~R), regardless of the chain length or grafting density¹⁵. So far there have been a limited number of studies devoted to a systematic investigation of the pore curvature effect on the properties of grafted polymers and in particular on chain conformation. The results of a self-consistent mean-field (SCMF) study showed that depending on the definition of brush height (e.g., using the first moment vs. the second moment of volume fraction distribution) it either decreases monotonically with a decrease in pore size or exhibits a maximum when chains start to reach the pore center.²¹ Similar observations of a non-monotonic dependence of the brush height on nanopore radius was observed in bead-string MD simulations and is expected based on the SCMF model in the strong stretching limit.²⁹ On the other hand, in Monte Carlo simulations of polymer-grafted nanopores it was found that pore curvature has a rather weak effect on the brush height at least in the range of large pore sizes studied.²² We note that these studies have not considered explicit solvent, which may affect polymer conformation, and will be one of the subjects investigated in this paper.

To date there have been only a very few studies of polymer grafted nanopores at the atomistic level with explicit solvent consideration, which allows investigation of the solvent distribution within the pore, its interactions with the pore surface and polymer solvation, which can affect the polymer conformation and grafted layer properties, especially in connection to the polymer length, grafting density and pore size. This is especially important for the polymers for which solubility relies on the ability to form hydrogen bonds with water.

Atomistic molecular dynamics simulations of Poly(N-isopropylacrylamide) (PNIPAM) grafted onto the interior of a carbon nanotube (with a radius comparable to the polymer size) at a low grafting density as a function of the temperature, surface-polymer interaction strength and pore water content have been carried out for the purpose of elucidating thermo-responsive control.³⁰ In this study a collapsed conformation of the polymer with diminished hydrogen bonding between the PNIPAM and water was observed upon a temperature increase above the PNIPAM lower critical solution temperature (LCST). In a very recent study, ^{1,31} by atomistic MD simulations the effects of the surface properties (hydrophilic vs. hydrophobic) of a carbon nanopore on the grafted PEG conformation and ion transport have been studied. It was found that the presence of urea results in a slightly more compact conformation of PEG which in turn affects the ion transport within the pore, depending on the ion type. So far atomistic MD simulations have been limited to a low grafting density of polymers, and therefore explored only the mushroom regime.

In this paper we investigate by means of atomistic MD simulations the structural and hydration properties of PEO grafted gold nanopores and systematically investigate the effects of grafting density, PEO length and pore curvature. In particular, we aim to explore the pore curvature effect on the PEO conformation within the pore and the properties of the grafted PEO layer. The obtained results will also be compared to that for PEO grafted planar^{32,33} and convex spherical surfaces^{34–36}. Our results provide a molecular picture of the local chain/water arrangement, polymer conformation and hydration, which is essential for both fundamental understanding of macromolecular behavior under confinement and practical applications like nanopore-gated control devices.

SIMULATION DETAILS

We have performed all-atom molecular dynamics simulations of PEO-grafted gold nanopore of varying pore sizes, PEO chain length, and grafting densities. All simulations were carried out using the GPU accelerated Gromacs version 2020.437 on the Extreme Science and Engineering Discovery Environment (XSEDE).³⁸ The gold nanopore was constructed using the fcc lattice with a lattice constant of 4.08 Å, with the force field adopted from the literature,³⁹ and which was also used in the previous simulations of planar and spherical PEO brush^{32,34,35} by one of us. The gold nanopore radius R was varied from 2.0 to 6.0 nm. The force field parameters of PEO and the van der Waals interactions were the same as in previous PEO brush studies.^{32,34,35} We studied PEO with the number of repeat units (*N*) 12, 20, 26, and 36. The PEO chains were approximately homogeneously end-grafted to the gold nanopore inner surface via sulfur bonds of thiol-terminated PEO (-S-CH₂-CH₂-[O-CH₂-CH₂]_N-O-CH₃). The parameters for the sulfur atom are from the standard OPLS-AA force field.⁴⁰ The PEO grafting density, *i.e.*, the number of chains per unit area, was varied (depending on chain length) from $\sigma = 0.30 \text{ nm}^{-2}$ to $\sigma = 1.20 \text{ nm}^{-2}$. In all simulations the SPCE water model⁴¹ was used. All simulations were performed at T=300K and pressure of 1 bar.

All systems were first energy minimized by the steepest descent algorithm, which was followed by a three-step equilibration protocol for at least 100 ns, as described in the Supporting Information. For the production run NPT simulations using the V-rescale thermostat (time constant of 0.1 ps) and the Berendsen barostat (time constant of 5.0 ps) were performed for at least 80 ns (for dense systems approximately 300 ns). The electrostatic interactions were calculated by the PME method with a Fourier spacing of 0.12

nm. All hydrogens were constrained using the LINCS algorithm such that a timestep of 2 fs was enabled. Periodic boundary conditions in all directions were applied. In all simulations Newton's equation of motion was integrated by the leap-frog algorithm.

To calculate the polymer volume fraction and hydrogen bond profiles the positions of atoms within a cylindrical shell of 0.4 nm width starting from the gold surface to the center of the pore were analyzed. The volume for the PEO and sulfur atoms were the same as our previous publications, 32,34,35 *i.e.*, 0.03 nm³ for water, 0.02 nm³ for PEO oxygen and $-CH_2/-CH_3$ group and 0.0236 nm³ for sulfur. The hydrogen bonds between water and PEO were determined based on a geometrical criterion for the distance between oxygens of water and PEO $r_{DA} \le 3.5$ Å and the angle \angle HDA $\le 30^\circ$ with H being a hydrogen atom of water, D the water oxygen atom (donor) and A the PEO oxygen atoms (acceptor). For the end-group distribution, we calculated the radial distance of the end group $-CH_3$ to the gold surface.

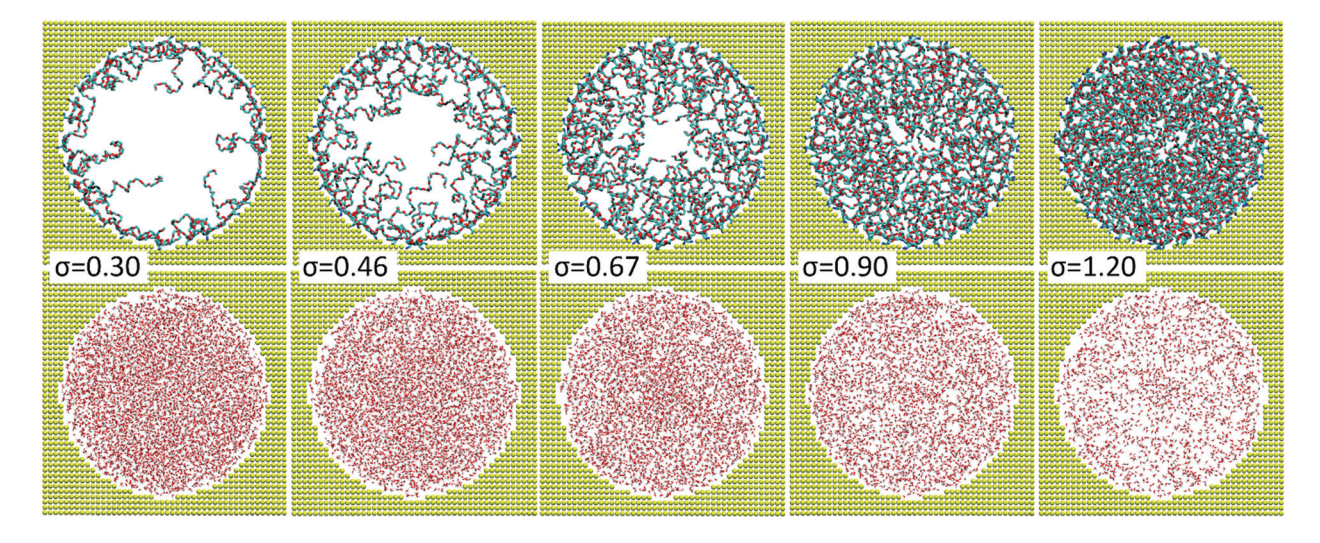


Figure 1: Cross-sectional MD simulation snapshots of a PEO-grafted gold nanopore of 4 nm radius at different grafting densities (0.30, 0.46, 0.67, 0.90, and 1.20 nm⁻² from the left to the right) for PEO of N=20 repeat units at T=300 K. Gold nanopores are shown in yellow, PEO backbone chains are represented as lines (top panel) and water molecules in red (bottom panel). The snapshots were produced using VMD.⁴²

RESULTS AND DISCUSSION

PEO Grafting Density Effect. Grafting density plays a crucial role in determining the properties of grafted polymer layers. We systematically investigated the effect of grafting density σ on the properties of PEO grafted to gold nanopores. As is seen in Figure 1 for a gold nanopore of 4nm radius, the equilibrated structure of grafted PEO layer varies from a dilute mushroom-like structure at low σ to a dense brush upon increasing the grafting density. One can also see that in the mushroom regime (e.g., 0.30 nm⁻² in Figure 1 for N=20) in a sufficiently large pore, PEO chains tend to adsorb on the gold surface replacing layered water, as in the case of PEO chains grafted on planar and spherical surfaces. 32,34,35 At higher grafting densities PEO chains become more stretched and have less tendency for surface adsorption as they orient away from the surface and eventually enter the brush regime. The change in the aspect ratio of end-to-end distance (R_{END}) to the radius of gyration (R_g) and the expansion ratio of the R_g to R_{g0} (in aqueous solution) with grafting density increase is consistent with this observation (Figure S1 in the Supporting Information). The aspect ratio increases with an increase of the grafting density and is comparable to PEO grafted on planar surfaces except at the highest grafting density where the aspect ratio is about 1.1 times that of polymers grafted on planar surfaces, indicating enhanced chain stretching. The expansion ratio of PEO at lower grafting densities ($\sigma \le 0.67$ nm⁻²) is comparable to planar surfaces.

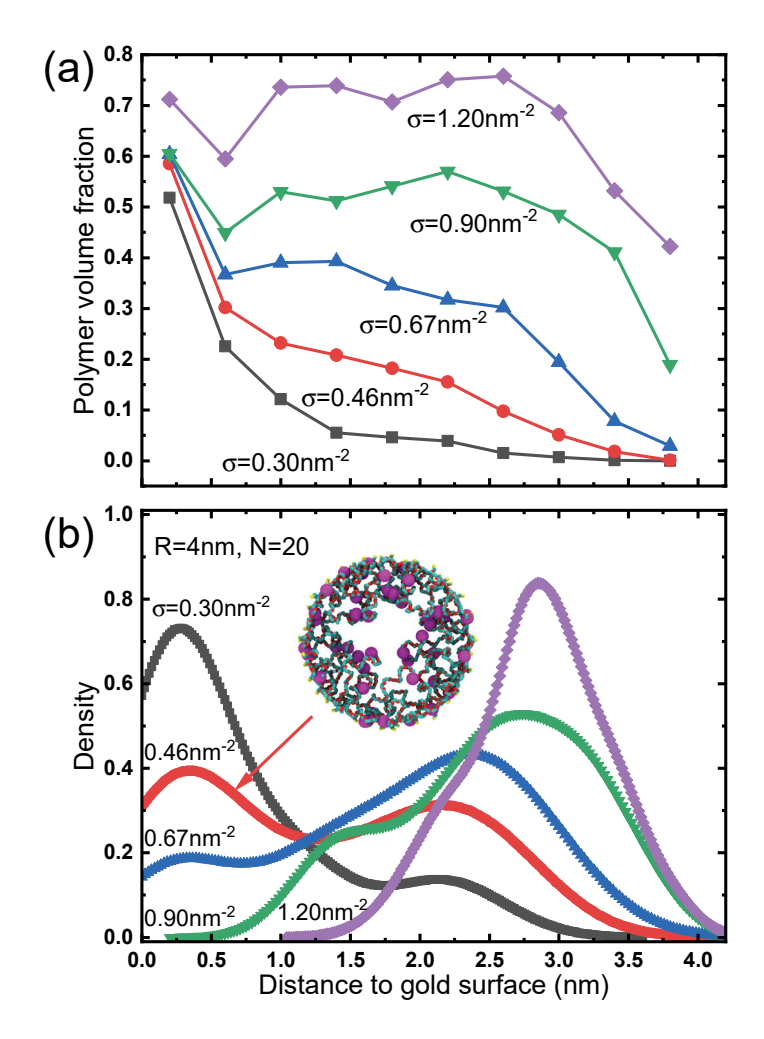


Figure 2: Polymer grafting density effects. (a) PEO volume fraction as a function of distance to the surface of a gold nanopore of 4nm radius grafted by PEO chains of 20 repeat units at different grafting densities: 1.2 nm^{-2} (diamonds), 0.90 nm^{-2} (down triangles), 0.67 nm^{-2} (up triangles), 0.46 nm^{-2} (circles) and 0.30 nm^{-2} (squares); (b) The end group distribution of the grafted polymer to the surface of gold nanopore of 4nm radius at different grafting densities: 0.30, 0.46, 0.67, 0.90, and 1.20 nm^{-2} . Inset: computer simulation snapshot for σ = 0.46 nm^{-2} showing the grafted polymer conformation and the end group (magenta beads) distribution.

To quantitatively characterize the structural properties of grafted polymer layers, we analyzed the volume fraction of PEO polymers as a function of the distance to the gold surface. The results for a gold nanopore of 4nm in radius grafted by PEO with a chain length of 20 repeat units for various grafting densities are shown in Figure 2(a). As can be seen, at low

grafting density (0.30 nm⁻²) the polymer volume fraction decreases quickly away from the surface, implying that polymer chains exclusively reside near the gold surface and there are no polymers that reach the pore center. As the grafting density increases polymer chains start to stretch out due to the excluded volume interactions and the volume fraction increases away from the gold surface, as can be seen in the snapshots shown in Figure 1. At the highest grafting density considered (1.20 nm⁻²), a step-like dependence is seen in Figure 2(a) with a high-volume fraction plateau value of 0.6. A similar density profile has also been observed (at high grafting density) in Monte Carlo simulations of coarse grained polymers grafted on the inner surface of cylindrical pores²² and atomistic MD simulations of a planar PEO brush.³² It is interesting to note that in all cases shown in Figure 2(a) the polymer volume fraction is high in the immediate vicinity of gold surfaces which is due to polymer adsorption on the surface at low grafting density and chain crowding at high grafting density. Similar behavior has also been observed in MD simulations of planar³² and spherical PEO brushes.34,35 In contrast to convex surfaces where volume available for polymer chains expands with increased distance from the surface, in the case of concave surfaces there is more volume near the surface, so there are pockets of water at approximately 0.6nm from the surface, as indicated by the polymer volume fraction plot (Fig. 2(a)).

The end-group density distribution provides a more direct indication of the structural properties of the PEO layer, as shown in Figure 2(b). At the lowest grafting density (0.30 nm⁻²) the majority of the end-groups reside in the vicinity of the gold surface, signaling chain adsorption. As the grafting density increases some chains with corresponding ends groups remain adsorbed on the surface, but other chains start to elongate away from the surface and a second peak of end group distribution at large distance from the surface is observed.

With an increase of grafting density chains become more crowded and the end-groups are distributed further away from the gold surface with the dominant peak value shifting towards the center of the gold nanopore. At the largest grafting density (1.20 nm⁻²), no polymer chain ends remain near the gold surface but are distributed within the nanopore interior with a peak value at about 2.85 nm from the surface. One can also see that the end group density does not vanish in the center at high grafting densities, suggesting that polymer fills the pore for $\sigma \ge 0.90$ nm⁻².

The hydration properties of the grafted PEO polymers are interconnected with the chain conformation and are important for practical applications, such as protein adsorption inhibition and solvent-induced gate control of pore opening/closing. In Figure 3(a) the average number of hydrogen bonds with water per PEO oxygen are shown as a function of the distance to the gold surface for different grafting densities. As can be seen, the average number of hydrogen bonds reaches 1.2 (expected for PEO in aqueous solutions⁴³) at low grafting density, $\sigma \le 0.46$ nm⁻², implying a well-hydrated state of the polymer, except in the vicinity of the gold surface (\sim 0.5 nm) where the polymer is adsorbed on the surface. With an increase of grafting density, the average number of hydrogen bonds formed between PEO and water decreases as PEO chains more densely pack, forming a brush. At the highest grafting density (1.20 nm⁻²), the average number of hydrogen bonds drops to 0.7, signaling a somewhat dehydrated state, as the polymer volume fraction significantly exceeds that of water. We note that at high grafting densities ($\sigma \ge 0.9 \text{ nm}^{-2}$), the average fraction of hydrogen bonds increases near the pore center indicating the higher volume fraction of water and accordingly higher polymer hydration.

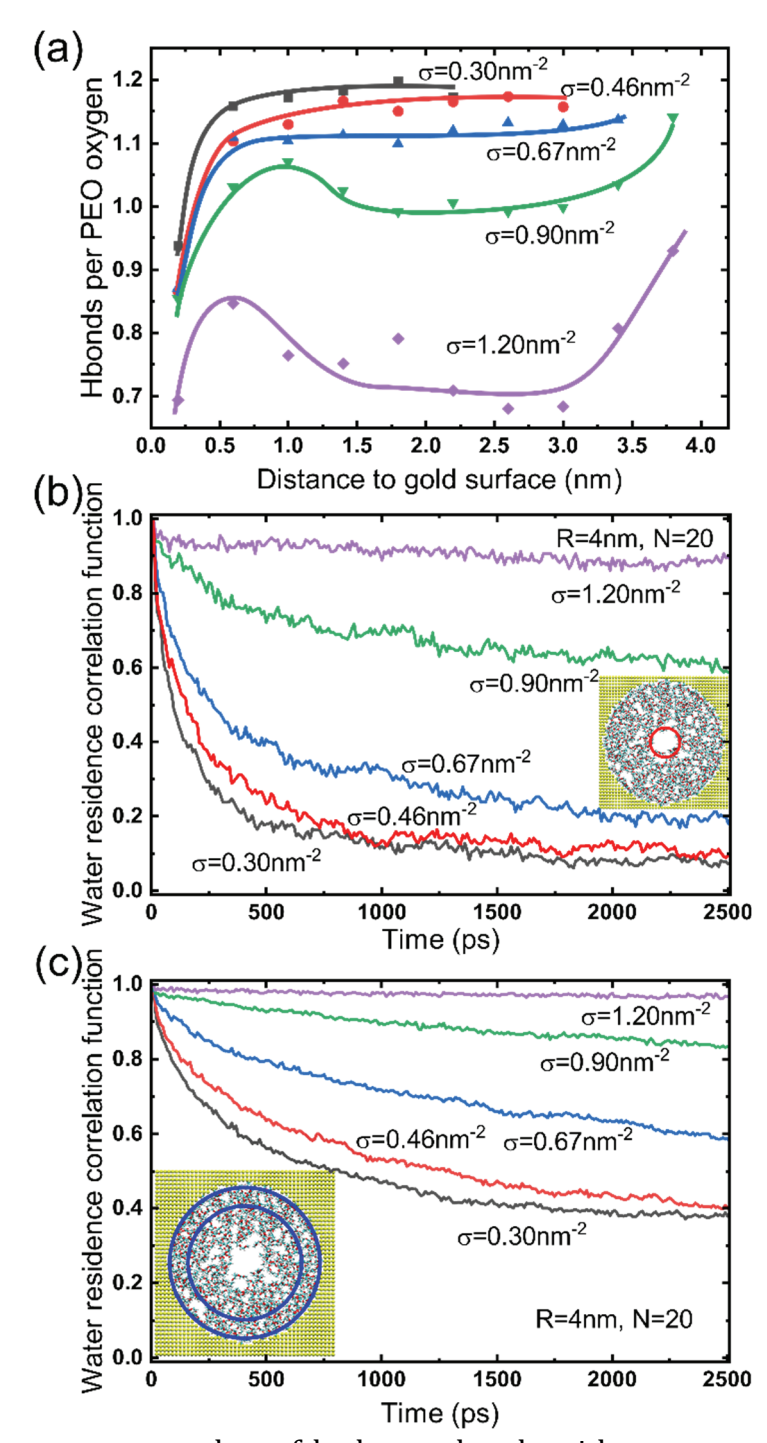


Figure 3: (a) The average number of hydrogen bonds with water per PEO oxygen as a function of the distance to the gold surface at different grafting densities: 1.20 nm⁻² (diamonds), 0.90 nm⁻² (down triangles), 0.67 nm⁻² (up triangles), 0.46 nm⁻² (circles) and 0.30 nm⁻² (squares); (b-c) Water residence correlation functions calculated using Eq. 1 for the water located within 1 nm of the center for a nanopore (b) and the water located within 1 nm of the nanopore surface (c) of radius 4 nm grafted by PEO chain of 20 repeat units

(N=20) at different grafting densities: 0.30, 0.46, 0.67, 0.90 and 1.20 nm⁻²; Insets in b) and c) for σ =0.67 nm⁻² show the 1nm region near the nanopore center (b) or surface (c) for which correlation functions were calculated.

In polymer-grafted nanopore-based transportation and control applications solvent mobility within the pore and especially the pore center is of practical importance. To examine this property and its dependence on grafting density, we carried out an analysis of the water residence correlation function (C(t)) within 1 nm of the pore center and within 1nm of the pore surface:

$$C(t) = \langle \frac{N_w(t)}{N_w(0)} \rangle \tag{1}$$

where $N_w(0)$ is the number of waters at time zero and $N_w(t)$ the number of waters remaining in the shell at time t. As is seen in Figure 3(b), at low grafting densities (0.30 nm⁻² to 0.46 nm⁻²), the center of the pore is open, and water is very mobile with most of the water exchanged within 0.5ns. Fitting the water residence correlation data with a biexponential function shows that the initial decay occurs with an effective lifetime of ~200ps at low grafting densities (Table S2 of Supporting Information). As the grafting density increases, the open portion of the pore starts to shrink as the polymer expands towards the pore center (Figure 1). This slows down the water exchange with the decay time increasing nearly 10-fold and at high grafting densities (larger than 0.90 nm⁻²), more than 70 percent of original water remains within 1nm from the pore center after 2ns. At the highest grafting density considered (1.20 nm⁻²) the water is practically stagnant, consistent with the visually observed closed pore (Figure 1).

In contrast, water mobility near the gold surface is much slower than that in the nanopore center at the same grafting density, as shown in Figure 3(c). The initial decay of water near the nanopore surface is at least twice slower compared to that at the center for all grafting densities considered (Table S2 of Supporting Information). With an increase of grafting density water exchange near the surface slows down more significantly than at the pore center by a factor of 4. Two main factors contribute to this effect: a higher polymer volume fraction and water layering near the nanopore surface, both of which slow down the water exchange.

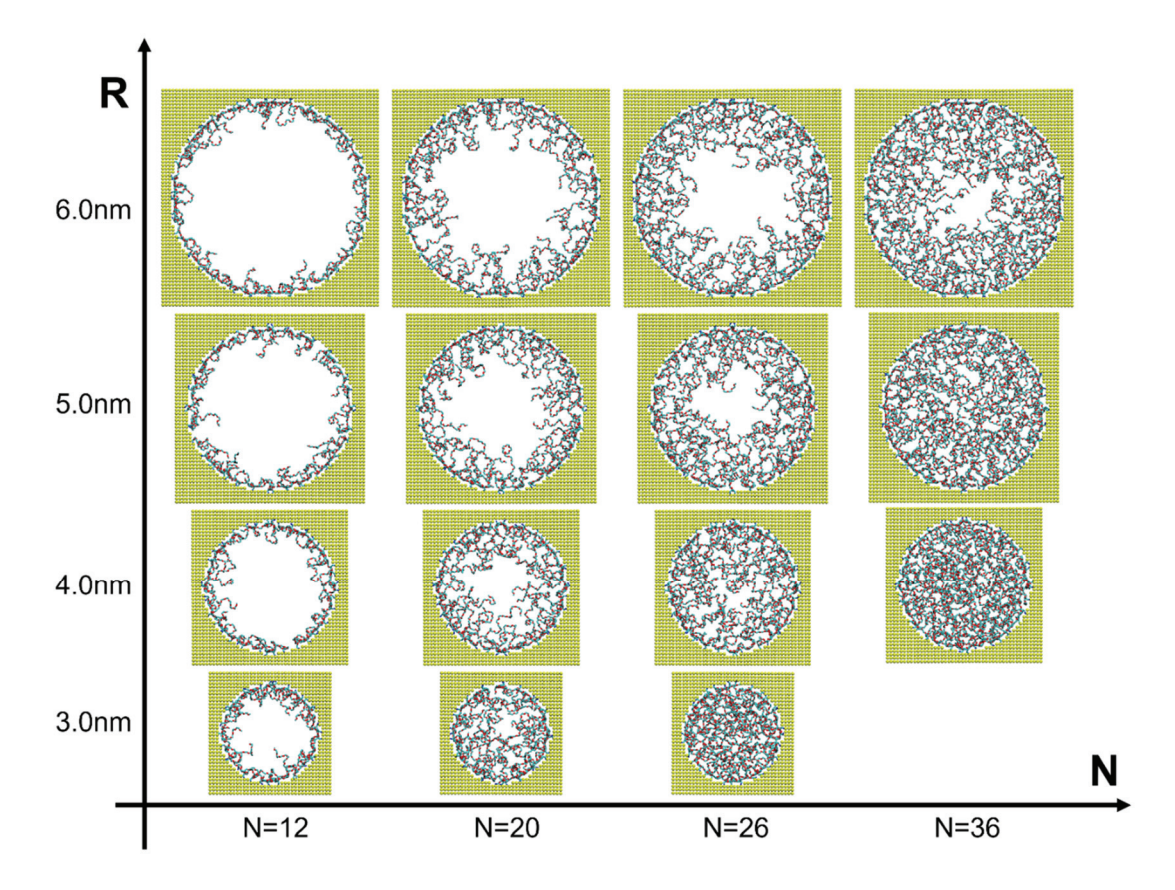


Figure 4: Cross-sectional MD simulation snapshots of PEO-grafted gold nanopores of different sizes with a grafting density of 0.46 nm⁻² for PEO chains with different numbers of repeat units N at T=300 K. Gold nanopores are shown in yellow, and PEO backbone chains are represented as lines. The snapshots were produced using VMD.⁴²

PEO Chain Length Effect. Another factor which strongly influences the properties of grafted polymer layers is chain length. At a given grafting density short polymer chains may be in a mushroom regime, while longer chains start to overlap on the surface and with a further increase of chain length form a dense brush. To investigate the interplay of the chain length and nanopore size effect, we held the grafting density constant at 0.46 nm⁻² and varied the length of grafted PEO chains: N=12, 20, 26, and 36 for nanopores of different radii: 3, 4, 5 and 6 nm. Computer simulation snapshots of equilibrated structures are shown in Figure 4. As is seen for the shortest chains, polymers are in the mushroom regime and adsorb on the gold surface (Figure 5a), as discussed above. As the chain length increases, polymers are stretched out from the gold surface towards the pore center forming a brush, which eventually fills the whole pore.

The polymer volume fraction profiles are shown in Figure 5(b) for a nanopore of 4nm radius. For the shortest chain length, PEO chains are mainly adsorbed on the surface with the polymer volume fraction rapidly decreasing away from the gold surface. Accordingly, the end-group distribution (Figure S2 in the Supporting Information) shows than the majority of chain ends reside near the gold surface and polymers remain well-hydrated (Figure S3), except in the very vicinity of the surface. An increase in chain length results in a broader polymer volume fraction distribution as the chains start to overlap and extend away from the surface (Figures 5a-b) and the end-group distribution becomes broader and bimodal with some chains ends remaining in the surface vicinity but with the majority of the chains ends extending towards the pore center (Figure S2 in the Supporting Information). For the longest chain length considered (N=36) the polymer volume fraction levels off at about 0.5 throughout the pore and hydrogen bonding decreases (by 12-15%) except for the vicinity of

the gold surface, where some chain adsorption (with a low level of hydration) still occurs. The end-group distribution remains broad with a shallow maximum located within the middle of the grafted layer in agreement with results of CGMD simulations for polymer grafted nanopores.¹⁷

Comparing the effect of grafting density (Figure 2a) and chain length (Figure 5b) increase for a given pore size, one observes a qualitatively similar trend: the monomer density in the pore interior increases with grafting density or chain length increase. In both cases polymers stretch away from the surface due to chain crowding resulting in a somewhat dense brush which can fill the whole pore, depending on polymer chain length and grafting density. At the same time, it is important to note the effect of chain length and grafting density are not interchangeable: e.g. an increase in grafting density (for a given chain length) can lead to chain stretching, while an increase in chain length (for a given grafting density) may not (Figure S4). In general, significant differences in chain conformation and polymer distribution are achieved by PEO chains of different lengths and grafting densities, especially when surface curvature comes into play, which will be discussed below.

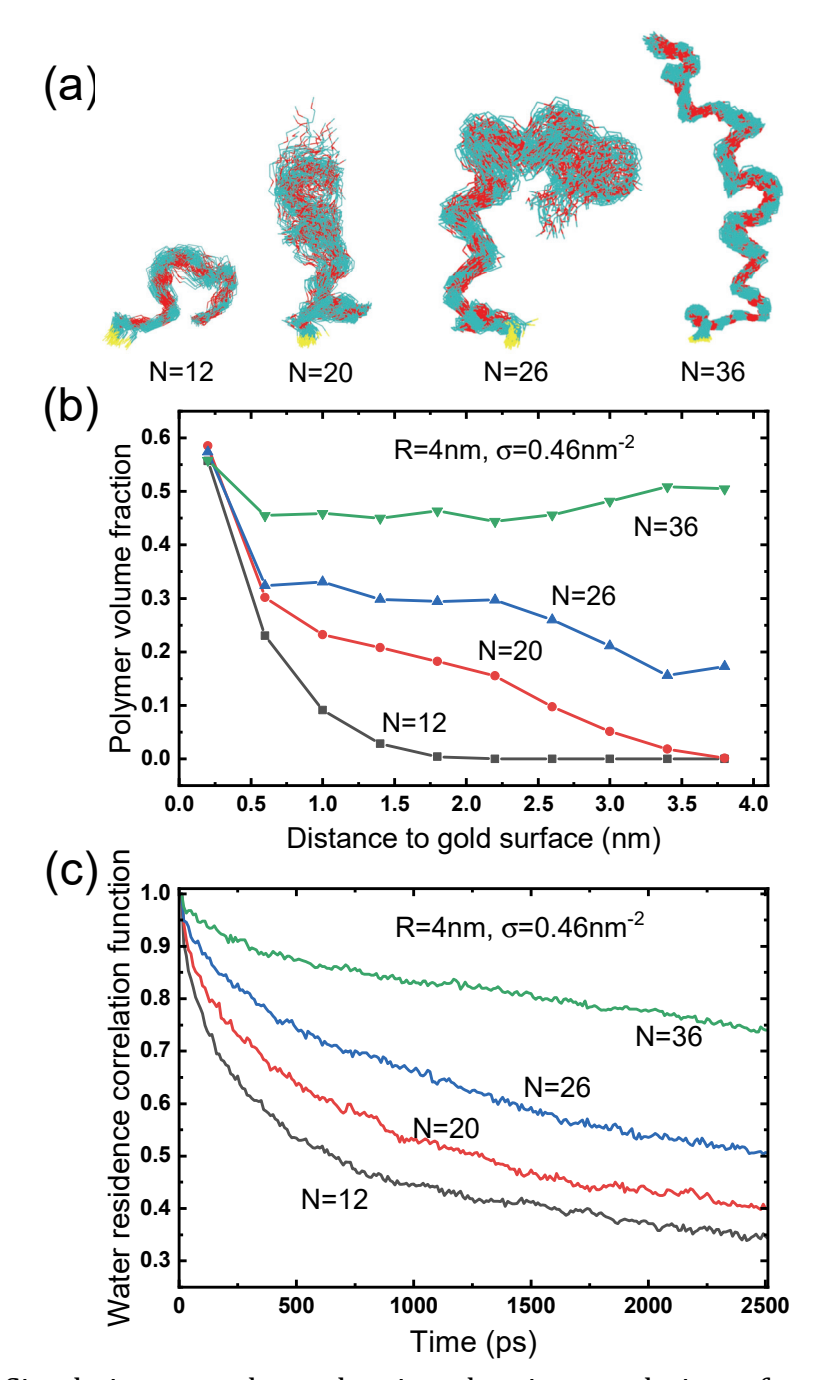


Figure 5: (a) Simulation snapshots showing the time evolution of typical PEO chain conformation for different PEO chain lengths N=12, 20, 26 and 36 grafted with 0.46 nm⁻² grafting density to the gold nanopore of 4nm radius (b) Polymer volume fraction as a function of the distance to the surface of gold nanopore of 4nm radius grafted by PEO chains with different number of repeat units: N=12 (squares), 20 (circles), 26 (up triangles) and 36 (down triangles) at a grafting density of 0.46 nm⁻²; (c) water residence correlation functions calculated using Eq. 1 for the water located within 1 nm of the nanopore surface.

The water residence correlation function for water within 1nm of the nanopore surface calculated using Eq. 1 is shown in Figure 5(c). Even though the polymer volume fraction at the surface is nearly the same (Figure 5b), one can see that water exchanges considerably quicker for the nanopores grafted by shorter polymer chains with an effective exchange time of 550ps. The main reason for this behavior is that away from the surface the polymer volume fraction decreases considerably faster for shorter chains (e.g., N=12), while for longer chains (N=36) it remains at nearly the same level thereby slowing down the water exchange. In all cases, the water exchange near the nanopore surface occurs 2-4 time more slowly than at the nanopore center (Table S3 and Figure S5 of Supporting Information), where the volume fraction of water is higher. It is also interesting to note the differences in the chain mobility for different chain lengths, as illustrated by time span of conformations shown in Figure 5a. One could expect that the shortest chains (N=12) could be the most mobile, but this is not the case: chain adsorption to the nanopore walls (replacing layered water) diminishes chain mobility and chain conformation changes very little despite the quick water exchange near the surface (Figure 5c). With an increase of chain length, only a small portion of the chain remains near the surface and the rest of the chain changes conformation freely (Figure 5a). A further increase in chain length results in an increase of polymer density in the grafted layer, which in turn slows down chain mobility, especially when chains start to fill the pore (N=36).

To quantify the thickness of the grafted polymer layers, we calculated using cylindrical coordinates brush height based on the polymer volume fraction:^{12,21,22}

$$H = 3 \frac{\int_0^R (R - r) \Phi(r) r^2 dr}{\int_0^R \Phi(r) r dr}$$
 (2)

where $\Phi(r)$ is the polymer volume fraction at the radial distance r from the pore center and R is the pore radius.

One can see that Eq. 2 takes into account the curvature effect of the cylindrical nanopore and the coefficient 3 originates from the normalization of the brush height for a constant polymer density. We note that the first moment integration of the volume fraction ($H_p = \int_0^R (R-r)\Phi(r)dr/\int_0^R \Phi(r)dr$) has been applied for brush height estimation.^{11,21} However, this expression does not account for cylindrical symmetry of the system studied here and is commonly applied for a planar brush geometry. Therefore, we choose to use Eq. 2 for the polymer brush height calculation.

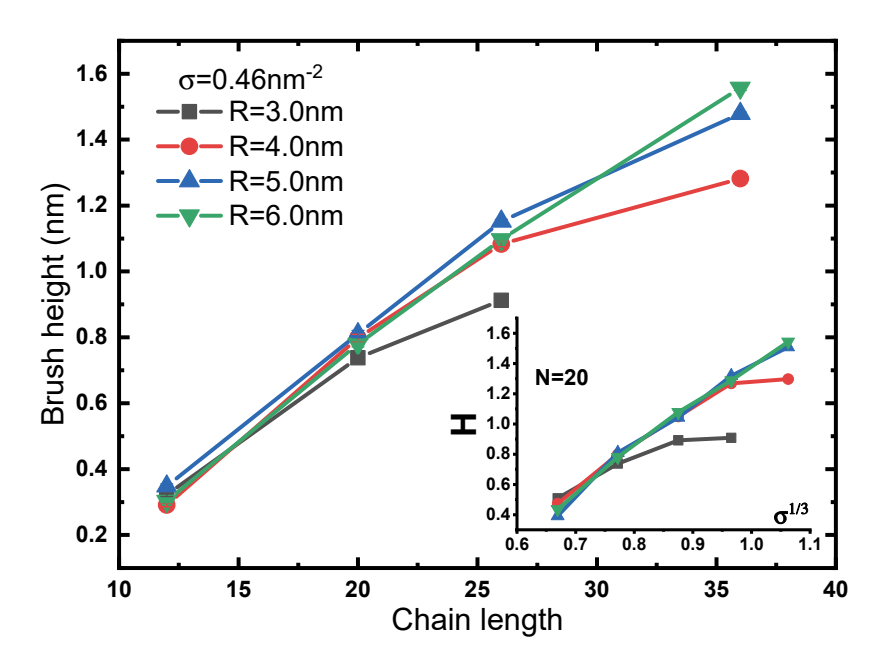


Figure 6. Polymer brush height as a function of the number of PEO repeat units, N, at the grafting density of 0.46 nm⁻² for different pore radii. Inset is the brush height as a function of $\sigma^{1/3}$ for PEO chain length N=20 for different pore sizes.

The polymer brush height as a function of the chain length is plotted in Figure 6. As is seen, the brush height follows a nearly linear dependence on the chain length H \sim N, as was previously reported in coarse grained MD simulations,¹⁷ self-consistent field predictions^{14,21} of polymers grafted to concave nanopores and as expected for planar brushes.⁴⁴ However we note that for longer chain lengths there is a deviation from this linear dependence, which is related to confinement effects, as will be discussed below and was previously reported in a Monte Carlo study of coarse grained polymers grafted to nanopores²² where the brush height H was found to follow a $N^{0.84}\sigma^{0.26}$ dependence (chain length N in 30~100). We also analyzed the brush height dependence on the grafting density, as shown in inset of Figure 6. While our data are consistent with $\sigma^{1/3}$ scaling expected for planar brush⁴⁴ and observed in coarse grained MD simulations¹⁷ and self-consistent field predictions^{14,21} of polymers grafted in nanopores, it is hard to definitively support it, as high grafting densities cannot be attained for the small nanopores studied here due to confinement effects, as discussed below.

Nanopore Curvature Effect. The pore size/curvature has the most complicated influence on the structural and hydration properties of the grafted polymers as the accessible volume is drastically decreasing from the pore surface towards the pore center. Figure 7 shows the volume fraction of PEO (N=20) grafted to nanopores of different radii with the same grafting density 0.46 nm⁻². As is seen, in the narrow pores, polymer chains are highly crowded and fill the whole pore (Figure 4) with a volume fraction reaching 0.4-0.5 for R= 2.5 and 2.0 nm (Figure 7). The PEO volume fraction can even reach up to 0.8 for R=3.0nm and R=4.0 nm at a higher grafting density of 0.90 nm⁻² and 1.20nm⁻², respectively (Figure S6 in the Supporting Information). In all cases, with an increase of pore size, the volume fraction decreases away from the surface (Figure 7), leaving a polymer-free region near the pore center (Figure 4).

This implies that the critical polymer grafting density σ^* for the mushroom to brush transition depends not only on polymer size, *i.e.*, radius of gyration in solution, $R_{g0} \sim N^{3/5} l$ (in a good solvent with l being the segment length), but also on nanopore curvature. Considering the overlap of grafted chains not just on the surface, but at distance R_g from the surface, we arrive at the following relation for σ^* :

$$\sigma^* \cong \frac{1}{R_{g0}} \left(\frac{1}{R_{g0}} - \frac{1}{R} \right). \tag{3}$$

Eq. 3 accounts for both the chain length and the nanopore curvature and should be applicable when $R_{g0} < R$. It implies that a polymer grafted to smaller nanopores experiences a larger effective grafting density, $\sigma_{\rm eff} = \sigma/(1 - R_{g0}/R)$ on account of being more crowded inside the pore. As the pore size increases such that $R \gg R_{g\theta}$ the contribution of surface curvature becomes negligible, and we approach the limit of a flat surface $\sigma^* \sim 1/R_{g0}^2$, where the chain overlap is affected only by chain length, (e.g., in a good solvent $R_{\rm g0}^2 \sim N^{6/5} l^2$). Indeed, comparing the polymer volume fraction profile obtained for PEO grafted to a planar gold surface³² at the same grafting density 0.46 nm⁻² (Figure 7), we notice that volume fraction profiles obtained for a pore of R=5nm>> $R_{g0}\approx2.4$ nm is only somewhat larger than that for the planar brush. Furthermore, compared to spherical nanoparticles grafted with PEO of the same length^{34,35} and at the same grafting density (0.46 nm⁻²) one can notice that the polymer density decays even faster away from the surface for spherical nanoparticles of higher curvature, as the space available for chains expands and the effective grafting density decreases³⁵ as $\sigma_{\rm eff} = \sigma/(1+R_{g0}/R)^2$. In contrast, for concave nanopores, we find that the effective grafting density that chains experience increases with an increase of curvature as $\sigma_{\rm eff} = \sigma/(1 - R_{g0}/R)$, since the space available to chains diminishes with distance away from the surface.

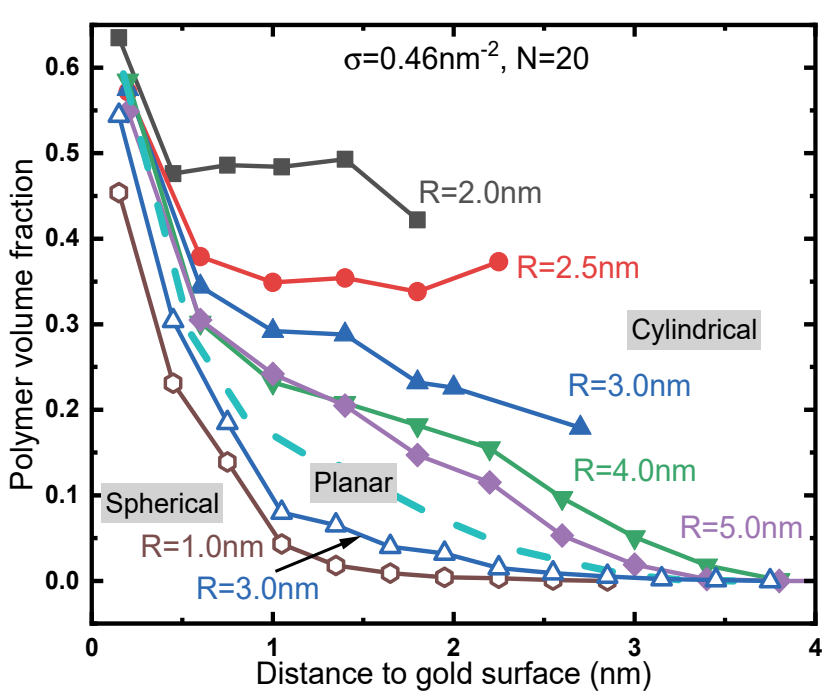


Figure 7: Polymer volume fraction as a function of the distance to the gold surface for surfaces of different curvature: spherical (open symbols) of radius 1nm (open hexagons), and 3nm (open triangles); planar (dashed line) and nanopores of radius 2 nm (squares), 2.5nm (circles), 3nm (up triangles), 4nm (down triangles), 5nm (diamonds) grafted with PEO chains of 20 repeat units (N=20) with grafting density of 0.46 nm⁻².

The average height of grafted PEO chains was calculated using Eq. 2 and is plotted in Figure 8 as a function of nanopore radius. As discussed above, for a given PEO chain length and pore size the average height of grafted chains increases with an increase in grafting density. As to the effect of pore size on the height for a given PEO length and grafting density, one can see that brush height remains at approximately the same level for sufficiently wide pores, i.e., for $R \gg R_{g0}$, in agreement with results of MC and bead-spring MD simulations. As the nanopore size becomes comparable to the polymer, *i.e.*, $R \approx R_{g0}$, polymers fill the whole pore and the height of grafted chains becomes limited by the available space, *i.e.*, nanopore size $H \sim R$. We observe this pattern for different grafting densities and chain lengths. For a given PEO length the critical pore size at which the limit $H \sim R$ is reached

systematically increases with grafting density, as chains are more stretched and fill the correspondingly larger pore. Similarly, longer PEO chains reach the limit $H \sim R \approx R_{g0}$ at a larger pore size. As the effective grafting density is affected by the curvature of the nanopore, as described by Eq. 3, a somewhat more complex dependence of grafted polymer height on pore radius can be observed for a low grafting density of polymer $\sigma < 1/R_{g0}^2$. In such cases, for large pores a mushroom regime with $H \sim R_{g0}$ is expected. With a decrease in the pore size, chain crowding can lead to the transition from the mushroom to brush regime and a corresponding increase in brush height. With further decrease in pore size chains start to fill the pore and the limit $H \sim R \approx R_{g0}$ is reached. In this scenario, the height would firstly increase, reach a plateau, and then decrease with a decrease of the pore size, such as we observed for PEO with N=20 for the grafting density 0.30 nm⁻² (Figure 8).

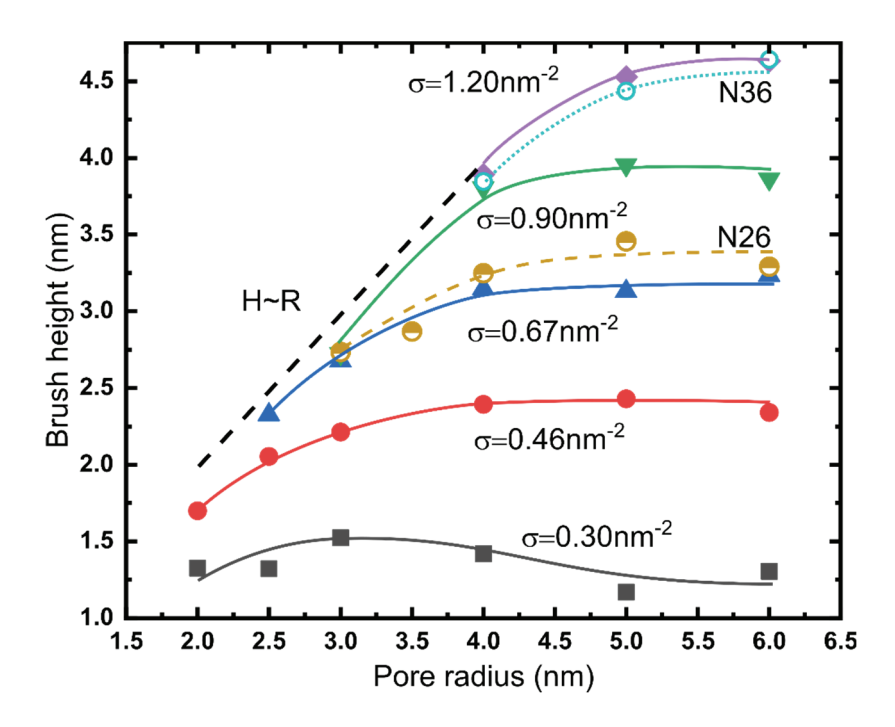


Figure 8: The average height (calculated using Eq. 2) of grafted PEO chains of different lengths as a function of the nanopore radius at different grafting densities: N=20 (σ =0.30 nm⁻² squares, σ =0.46 nm⁻² circles, σ =0.67 nm⁻² up triangles, σ =0.90 nm⁻² down triangles, and

 σ =1.20 nm⁻² diamonds), N=26 (σ =0.46 nm⁻² half-open circles, dashed line), N=36 (σ =0.46 nm⁻² open circles, dotted line).

To understand the molecular details of the PEO chain conformation in grafted polymer layers of different curvature (i.e., nanopore size), we analyzed chain stretching, orientation, shape, and hydration. As is seen from the computer simulation snapshots shown in Figure 9a-b for a grafting density of σ =0.90 nm⁻² for large pores (R= 4 and 5 nm) the PEO chains are stretched and radially oriented within the brush with an expansion ratio of about 1.1 (Figure 9c), similar to that for planar brush (Figure S1 in the Supporting Information). Having a relatively high polymer density within the brush, chains are somewhat less hydrated than in solution (Figure S7 of the Supporting Information). In contrast, for smaller pores (R=3nm), i.e., higher pore curvature at the same grafting density, PEO chains are not stretched, but rather slightly compressed (Figure 9b-c) due to confinement, forming a cone-like conformation to adjust to the available space. While the overall chain orientation remains radial, there is local chain folding and orientation along the pore surface, especially in the vicinity of the pore surface (Figure 9b and Figure S8 in the Supporting Information). The chain shape can be characterized by the asphericity parameter describing the degree of deviation of the chain shape from a sphere. It shows that when grafted to a low curvature surface, PEO chains are closer to a rod-like shape within the brush, while within a narrower pore they assume a more coil-like shape (Figure 9b and Figure S9 in the Supporting Information). The strong confinement effect in narrow pores means that the volume fraction of water is low, and the polymer is also noticeably dehydrated (Figure S7 of the Supporting Information) and chain mobility is low (Figure 9b). The overall pattern of chain conformational behavior with a change of pore curvature remains the same for different grafting densities, except for higher hydration and lower chain stretching and orientation for chains grafted at lower grafting densities on pores of larger sizes (Figure 9c and Figure S8 in the Supporting Information).

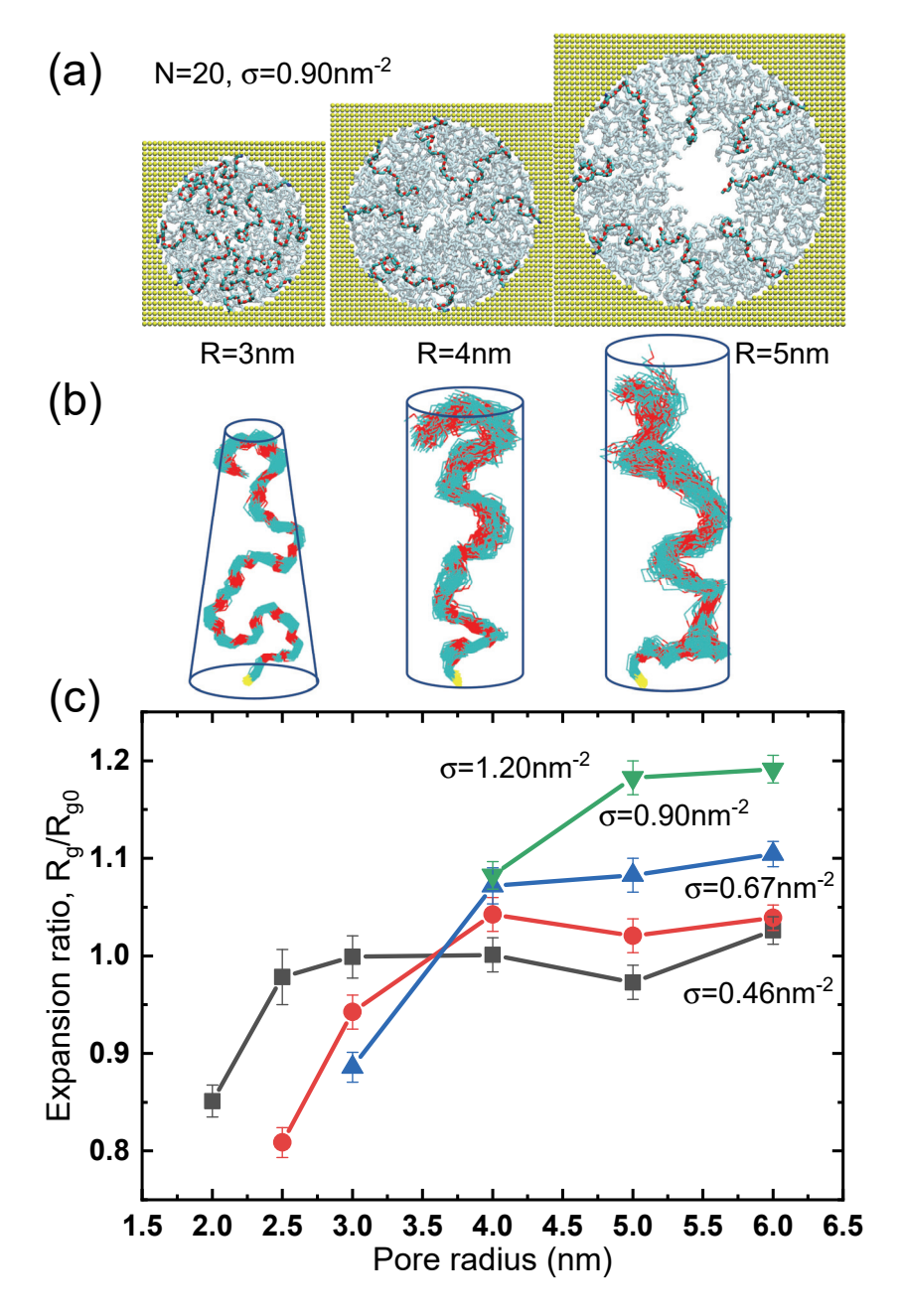


Figure 9: (a) Cross-sectional MD simulation snapshots showing chain conformation of PEO-grafted nanopores for different pore sizes (R=3, 4, and 5 nm) for chain length N=20 and grafting density σ =0.90 nm⁻², (b) Simulation snapshots showing the time evolution of typical PEO chain conformations and polymer volume shape for different pore sizes (R=3, 4, and 5 nm) for chain length N=20 and grafting density σ =0.90 nm⁻², (c) PEO expansion ratio R_g/R_{g0}

as a function of pore radius for different grafting densities: σ =0.46 nm⁻² (squares), σ =0.67 nm⁻² (circles), σ =0.90 nm⁻² (up triangles) and σ =1.20 nm⁻² (down triangles).

Diagram of states. To summarize the different regimes of behavior of grafted polymer chains inside the nanopore, we present in Figure 10 snapshots of PEO-grafted nanopores of varying pore size R and grafting density σ for PEO of 20 repeat units (N=20). At low grafting densities, when the pore size R well exceeds R_{g0} , i.e., R>> R_{g0} , grafted polymers are in the mushroom state and the pore is open (region I). As discussed above, chains have a tendency to adsorb on gold surface to replace layered water, thus it can be viewed as a pancake/mushroom regime. As grafting density increases (while $R >> R_{g0}$) grafted chains start to overlap (region II) and the height of the grafted layer increases, but chains remain mostly unstretched H $\sim R_{g0}$. The transition between mushroom to *overlapping chains* regime occurs according to Eq. 3 at the critical grafting density $\sigma^* \cong \frac{1}{R_{g0}} \left(\frac{1}{R_{g0}} - \frac{1}{R} \right)$. Using the coil dimension of PEO (N=20) in aqueous solution of about 2.4 nm,35 the curve corresponding to Eq. 3 is shown in Figure 10 as the boundary of the mushroom regime. At even higher grafting densities, PEO chains start to stretch and form a brush regime (region III) with the brush height increasing in a manner consistent with analytical predictions $H\sim N\sigma^{1/3}$ (the planar limit⁴⁴). While in the mushroom/pancake and overlapping grafted chain regimes PEO chains remain well-hydrated, this is not the case in the brush regime where the hydration shell is incomplete and degree of hydrogen bonding with water is less than that in aqueous solutions.

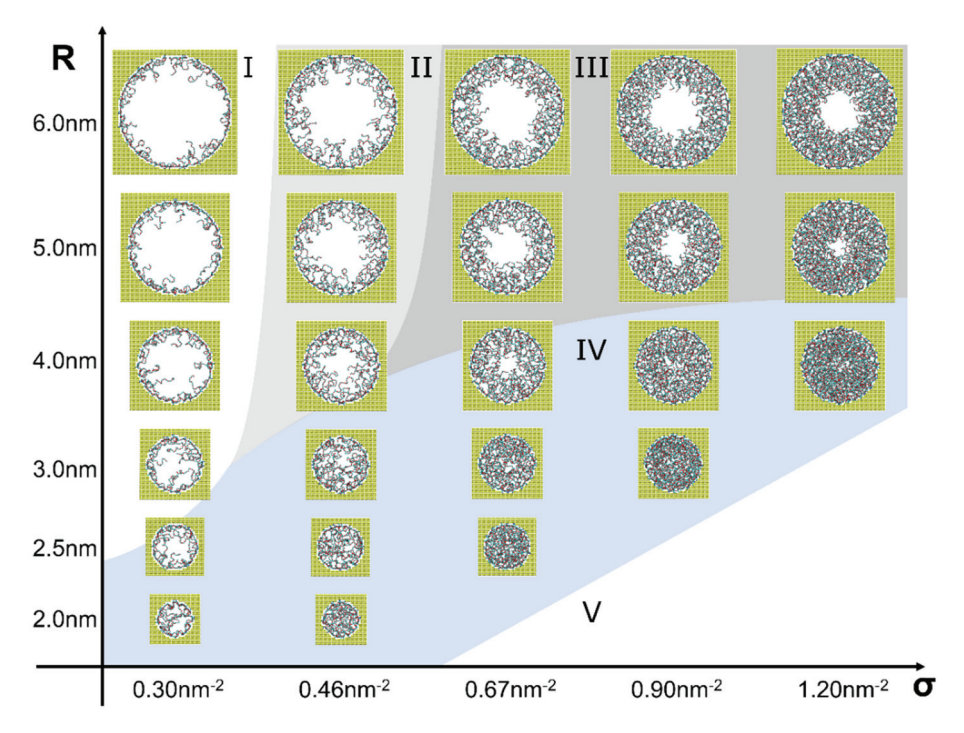


Figure 10: Schematic diagram showing simulation snapshots and different regimes of behavior of PEO chains of 20 repeat units grafted to nanopores: mushroom (region I), overlapping grafted chains (region II) and brush (region III) with the boundary between regions I and II given by Eq. 3. The closed pore region is indicated (region IV) as well as the restricted region where higher grafting density is hard to achieve on small pores (region V).

Another structural feature that is important for practical applications is whether the polymer-grafted nanopore is open or closed (region IV) with the criteria given by R \sim H. For mushroom/pancake and overlapping grafted chain regimes the nanopore remains open if R>H \sim R $_{g0}\sim$ N $_{g0}\sim$

having a high grafting density yields dehydrated chains with a polymer volume fraction that can be very high approaching 1 at small R, beyond which polymer grafting becomes impossible (region V).¹¹ The properties of closed pores with relatively low (weakly closed pore) and high polymer volume fraction (densely closed pore) are obviously different with respect to polymer hydration and transport properties, such as water exchange (Figure S10 in the Supporting Information).

CONCLUSIONS

Using atomistic molecular dynamics simulations, we have systematically investigated the structural and hydration properties of PEO grafted gold nanopores varying grafting density, chain length, and pore sizes. We found that for a given chain length and pore size, the grafting density controls the properties of grafted PEO layers. At very low grafting density, PEO tends to adsorb on the gold surface to alleviate water layering. As grafting density increases PEO forms a mushroom-like conformation with chain ends shifting towards to the pore center (Figure 2). At high grafting density polymer chains are densely packed in a brush and somewhat stretched and oriented along the radial direction. PEO chains are well hydrated at low and moderate grafting densities and become noticeably less hydrated as the grafting density further increases (Figure 3). Accordingly, water exchange near the pore center occurs quite rapidly at low grafting densities when the water dynamics are unobstructed by the polymer presence, while at high grafting densities when the polymer extends to the middle of the pore water exchange becomes stagnated (Figure 3). Water exchange near the nanopore surface is even slower than at the pore center due to the higher polymer density at the surface and water layering.

Increasing polymer chain length for a given grafting density and pore size results in structural changes from the mushroom conformation to overlapping grafted chains and stretched brush and can result in pore closure (Figures 4, 5). For a given grafting density water exchange occurs more rapidly for shorter chains grafted to the nanopore and noticeably slows down as chain length increases together with polymer volume fraction increase in the pore (Figure 5). Interestingly, chain conformations were more dynamically stagnant for the shortest and longest chains considered due to surface adsorption of the former and high polymer density within the pore for the latter (Figure 5). For open pores the brush height increases with chain length and grafting density in a manner consistent with expected scaling $H \sim N\sigma^{1/3}$ (Figure 6).²²

The nanopore curvature has strong effect on the properties of grafted PEO layers: decrease of pore size for a given grafting density and chain length results in a significant increase in polymer volume fraction and can lead to pore closure as well as polymer dehydration. This is a result of considerable polymer crowding within the pore, which translates into the higher effective grafting density for which we propose the relationship $\sigma_{\rm eff} = \sigma/(1 - R_{g0}/R)$. This curvature effect has to be taken into consideration if one wants to compare grafted polymer layers at the same grafting density for concave nanopores, planar and convex surfaces (Figure 7). For PEO grafted nanopores the increase of pore curvature, i.e. decrease in pore radius, does not significantly affect brush height as long as the pore size exceeds the polymer size (Rg). However, when the pore size becomes comparable to the brush height, H~R, the polymer chains fill the pore and start folding near the pore surface, forming a cone-shape and the brush height starts to decrease with decreasing pore size due to chain crowding (Figures 8, 9). For the case of low polymer grafting density

(mushroom/pancake regime) a decrease in pore size may result in an increase of layer height (overlapping mushroom regime) followed by the height decrease when the layer thickness reaches the pore radius (Figure 8). We anticipate that similar behavior can be expected for other water-soluble polymers, but details of behavior may differ depending on the degree of hydrophobicity of the polymer, its rigidity and capability for hydrogen bonding.

Our simulation results demonstrate different regimes of grafted PEO layers that can be achieved depending on grafting density, chain length and pore size: mushroom/pancake, overlapping mushrooms (with the height of the layer H~Rg0) and brush (Figure 10). Accordingly, the density of grafted layers changes from low to intermediate to high and the polymer hydration decreases from well-hydrated (as in aqueous solution) to somewhat dehydrated. Furthermore, polymer-grafted nanopores can be open or closed depending on whether the radius of the pore exceeds the height of the grafted layer or not. The properties of closed pores (e.g., water exchange in the pore center – Figure S10 in the Supporting Information) depends on the polymer density in the pore, e.g., whether the polymer conformation remains mushroom-like for a weakly closed pore or brush-like for a densely closed pore. Our results provide guidance for the design of polymer grafted nanopores with desired properties e.g., for gated control devices or separation membrane technologies.

ASSOCIATED CONTENT

Supporting Information:

The Supporting Information is available free of charge at https://pubs.acs.org/doi/...

Computer simulation system size and equilibration protocol; PEO expansion and aspect ratio, as functions of the grafting density; PEO end-group distribution for different chain length;

fitting parameters of a biexponential fit for different water residence correlation functions; chain expansion as the result of chain length or grafting density increase, the average number of hydrogen bonds with water and water residence correlation function at the nanopore center for PEO of different chain lengths; PEO polymer volume fraction as a function of the distance to the gold surface for different pore sizes; orientational order and asphericity functions of gold nanopore size for different grafting densities and water residence correlation function for closed pores of different polymer density.

AUTHOR INFORMATION

Corresponding Author:

Elena E. Dormidontova – Polymer Program, Institute of Materials Science and Physics Department, University of Connecticut, Storrs, Connecticut 06269, United States. Orcid: 0000-0002-7669-8957. Email: elena@uconn.edu

ACKNOWLEDGMENTS

This research is supported by the National Science Foundation under Grant No. DMR-1916864. This work used the Extreme Science and Engineering Discovery Environment (XSEDE) through allocation TG-MAT210004. XSEDE is supported by National Science Foundation grant number ACI-1548562.

REFERENCES

(1) Ma, T.; Arroyo, N.; Janot, J. M.; Picaud, F.; Balme, S. Conformation of Polyethylene Glycol inside Confined Space: Simulation and Experimental Approaches. *Nanomaterials*

- **2021**, 11 (1), 1–18, DOI 10.3390/nano11010244.
- (2) De Groot, G. W.; Santonicola, M. G.; Sugihara, K.; Zambelli, T.; Reimhult, E.; Vörös, J.; Vancso, G. J. Switching Transport through Nanopores with PH-Responsive Polymer Brushes for Controlled Ion Permeability. *ACS Appl. Mater. Interfaces* **2013**, *5* (4), 1400–1407, DOI 10.1021/am302820y.
- (3) Ma, T.; Walko, M.; Lepoitevin, M.; Janot, J. M.; Balanzat, E.; Kocer, A.; Balme, S. Combining Light-Gated and PH-Responsive Nanopore Based on PEG-Spiropyran Functionalization. *Adv. Mater. Interfaces* **2018**, *5* (2), 1–9, DOI 10.1002/admi.201701051.
- (4) Zhou, Y.; Guo, W.; Cheng, J.; Liu, Y.; Li, J.; Jiang, L. High-Temperature Gating of Solid-State Nanopores with Thermo-Responsive Macromolecular Nanoactuators in Ionic Liquids. *Adv. Mater.* **2012**, *24* (7), 962–967, DOI 10.1002/adma.201104814.
- (5) Yong, H.; Molcrette, B.; Sperling, M.; Montel, F.; Sommer, J. U. Regulating the Translocation of DNA through Poly(N-Isopropylacrylamide)-Decorated Switchable Nanopores by Cononsolvency Effect. *Macromolecules* **2021**, *54* (9), 4432–4442, DOI 10.1021/acs.macromol.1c00215.
- (6) Lim, R. Y. H.; Deng, J. Interaction Forces and Reversible Collaps of a Polymer Brush-Gated Nanopore. *ACS Nano* **2009**, *3* (10), 2911–2918, DOI 10.1021/nn900152m.
- (7) Perez Sirkin, Y. A.; Tagliazucchi, M.; Szleifer, I. Transport in Nanopores and Nanochannels: Some Fundamental Challenges and Nature-Inspired Solutions. *Mater. Today Adv.* **2020**, *5*, 100047, DOI 10.1016/j.mtadv.2019.100047.
- (8) Tagliazucchi, M.; Huang, K.; Szleifer, I. Routes for Nanoparticle Translocation through Polymer-Brush-Modified Nanopores. *J. Phys. Condens. Matter* **2018**, *30* (27), DOI 10.1088/1361-648X/aac90b.
- (9) Peleg, O.; Tagliazucchi, M.; Kröger, M.; Rabin, Y.; Szleifer, I. Morphology Control of Hairy Nanopores. *ACS Nano* **2011**, *5* (6), 4737–4747, DOI 10.1021/nn200702u.
- (10) Laktionov, M. Y.; Zhulina, E. B.; Richter, R. P.; Borisov, O. V. Polymer Brush in a

- Nanopore: Effects of Solvent Strength and Macromolecular Architecture Studied by Self-Consistent Field and Scaling Theory. *Polymers (Basel).* **2021**, *13* (22), DOI 10.3390/polym13223929.
- (11) Dimitrov, D. I.; Milchev, A.; Binder, K. Polymer Brushes in Cylindrical Pores: Simulation versus Scaling Theory. *J. Chem. Phys.* **2006**, *125* (3), DOI 10.1063/1.2211615.
- (12) Li, C. W.; Merlitz, H.; Sommer, J. U. Mean-Field Model of the Collapse Transition of Brushes inside Cylindrical Nanopores. *Macromolecules* **2020**, *53* (15), 6711–6719, DOI 10.1021/acs.macromol.0c00618.
- (13) Suo, T.; Shendruk, T. N.; Hickey, O. A.; Slater, G. W.; Whitmore, M. D. Controlling Grafted Polymers inside Cylindrical Tubes. *Macromolecules* **2013**, *46* (3), 1221–1230, DOI 10.1021/ma302302t.
- (14) Egorov, S. A.; Milchev, A.; Klushin, L.; Binder, K. Structural Properties of Concave Cylindrical Brushes Interacting with Free Chains. *Soft Matter* **2011**, *7* (12), 5669–5676, DOI 10.1039/c1sm05139c.
- (15) Emilsson, G.; Xiong, K.; Sakiyama, Y.; Malekian, B.; Ahlberg Gagnér, V.; Schoch, R. L.; Lim, R. Y. H.; Dahlin, A. B. Polymer Brushes in Solid-State Nanopores Form an Impenetrable Entropic Barrier for Proteins. *Nanoscale* **2018**, *10* (10), 4663–4669, DOI 10.1039/c7nr09432a.
- (16) Bayat, H.; Raoufi, M.; Zamrik, I.; Schönherr, H. Poly(Diethylene Glycol Methylether Methacrylate) Brush-Functionalized Anodic Alumina Nanopores: Curvature-Dependent Polymerization Kinetics and Nanopore Filling. *Langmuir* **2020**, *36* (10), 2663–2672, DOI 10.1021/acs.langmuir.9b03700.
- (17) Dimitrov, D. I.; Milchev, A.; Binder, K.; Heermann, D. W. Structure of Polymer Brushes in Cylindrical Tubes: A Molecular Dynamics Simulation. *Macromol. Theory Simulations* **2006**, *15* (7), 573–583, DOI 10.1002/mats.200600029.
- (18) Adiga, S. P.; Brenner, D. W. Flow Control through Polymer-Grafted Smart Nanofluidic Channels: Molecular Dynamics Simulations. *Nano Lett.* **2005**, *5* (12), 2509–2514, DOI

- 10.1021/nl051843x.
- Koutsioubas, A. G.; Spiliopoulos, N.; Anastassopoulos, D. L.; Vradis, A. A.; Toprakcioglu,
 C. Formation of Polymer Brushes inside Cylindrical Pores: A Computer Simulation
 Study. J. Chem. Phys. 2009, 131 (4), DOI 10.1063/1.3179686.
- (20) Binder, K.; Milchev, A. Polymer Brushes on Flat and Curved Surfaces: How Computer Simulations Can Help to Test Theories and to Interpret Experiments. *J. Polym. Sci. Part B Polym. Phys.* **2012**, *50* (22), 1515–1555, DOI 10.1002/polb.23168.
- (21) Suo, T.; Whitmore, M. D. Grafted Polymers inside Cylindrical Tubes: Chain Stretching vs Layer Thickness. *J. Chem. Phys.* **2013**, *138* (16), DOI 10.1063/1.4802632.
- (22) Viduna, D.; Limpouchová, Z.; Procházka, K. Monte Carlo Simulation of Polymer Brushes in Narrow Pores. *J. Chem. Phys.* **2001**, *115* (15), 7309–7318, DOI 10.1063/1.1405444.
- (23) Lee, J. H.; Lee, H. B.; Andrade, J. D. Blood Compatibility of Polyethylene Oxide Surfaces. *Prog. Polym. Sci.* **1995**, *20* (6), 1043–1079, DOI 10.1016/0079-6700(95)00011-4.
- (24) Awasthi, S.; Sriboonpeng, P.; Ying, C.; Houghtaling, J.; Shorubalko, I.; Marion, S.; Davis, S. J.; Sola, L.; Chiari, M.; Radenovic, A.; Mayer, M. Polymer Coatings to Minimize Protein Adsorption in Solid-State Nanopores. *Small Methods* **2020**, *4* (11), 1–10, DOI 10.1002/smtd.202000177.
- (25) Gon, S.; Kumar, K. N.; Nüsslein, K.; Santore, M. M. How Bacteria Adhere to Brushy PEG Surfaces: Clinging to Flaws and Compressing the Brush. *Macromolecules* **2012**, *45* (20), 8373–8381, DOI 10.1021/ma300981r.
- (26) Tagliazucchi, M.; Azzaroni, O.; Szleifer, I. Responsive Polymers End-Tethered in Solid-State Nanochannels: When Nanoconfinement Really Matters. *J. Am. Chem. Soc.* **2010**, *132* (35), 12404–12411, DOI 10.1021/ja104152g.
- (27) Wang, R.; Virnau, P.; Binder, K. Conformational Properties of Polymer Mushrooms under Spherical and Cylindrical Confinement. *Macromol. Theory Simulations* 2010, 19 (5), 258–268, DOI 10.1002/mats.200900085.

- (28) Sevick, E. M. Shear Swelling of Polymer Brushes Grafted onto Convex and Concave Surfaces. *Macromolecules* **1996**, *29* (21), 6952–6958, DOI 10.1021/ma9604552.
- (29) Eskandari Nasrabad, A.; Jasnow, D.; Zilman, A.; Coalson, R. D. Precise Control of Polymer Coated Nanopores by Nanoparticle Additives: Insights from Computational Modeling. *J. Chem. Phys.* **2016**, *145* (6), DOI 10.1063/1.4955191.
- (30) Alaghemandi, M.; Spohr, E. A Molecular Dynamics Study of Poly(N-Isopropylacrylamide) Endgrafted on a Model Cylindrical Pore Surface. *RSC Adv.* **2013**, 3 (11), 3638–3647, DOI 10.1039/c3ra22266g.
- (31) Arroyo, N.; Balme, S.; Picaud, F. Impact of Surface State on Polyethylene Glycol Conformation Confined inside a Nanopore. *J. Chem. Phys.* **2021**, *154* (10), DOI 10.1063/5.0040170.
- (32) Dahal, U. R.; Wang, Z.; Dormidontova, E. E. Hydration and Mobility of Poly(Ethylene Oxide) Brushes. *Macromolecules* **2017**, *50* (17), 6722–6732, DOI 10.1021/acs.macromol.7b01369.
- (33) Pop-Georgievski, O.; Verreault, D.; Diesner, M. O.; Proks, V.; Heissler, S.; Rypáček, F.; Koelsch, P. Nonfouling Poly(Ethylene Oxide) Layers End-Tethered to Polydopamine. *Langmuir* **2012**, *28* (40), 14273–14283, DOI 10.1021/la3029935.
- (34) Dahal, U.; Wang, Z.; Dormidontova, E. E. Hydration of Spherical PEO-Grafted Gold Nanoparticles: Curvature and Grafting Density Effect. *Macromolecules* **2018**, *51* (15), 5950–5961, DOI 10.1021/acs.macromol.8b01114.
- (35) Dahal, U.; Dormidontova, E. E. Chain Conformation and Hydration of Polyethylene Oxide Grafted to Gold Nanoparticles: Curvature and Chain Length Effect. *Macromolecules* **2020**, *53* (19), 8160–8170, DOI 10.1021/acs.macromol.0c01499.
- (36) Etame, A. B.; Smith, C. A.; Chan, W. C. W.; Rutka, J. T. Design and Potential Application of PEGylated Gold Nanoparticles with Size-Dependent Permeation through Brain Microvasculature. *Nanomedicine Nanotechnology, Biol. Med.* **2011**, *7* (6), 992–1000, DOI 10.1016/j.nano.2011.04.004.

- (37) Van Der Spoel, D.; Lindahl, E.; Hess, B.; Groenhof, G.; Mark, A. E.; Berendsen, H. J. C. GROMACS: Fast, Flexible, and Free. *J. Comput. Chem.* **2005**, *26* (16), 1701–1718, DOI 10.1002/jcc.20291.
- (38) Towns, J.; Cockerill, T.; Dahan, M.; Foster, I.; Gaither, K.; Grimshaw, A.; Hazlewood, V.; Lathrop, S.; Lifka, D.; Peterson, G. D.; Roskies, R.; Scott, J. ray; Wilkins-Diehr, N. Accelerating Scientific Discovery. *Comput. Sci. Eng.* **2014**, *16* (5), 62–74, DOI 10.1109/MCSE.2014.80.
- (39) Tay, K. A.; Bresme, F. Wetting Properties of Passivated Metal Nanocrystals at Liquid-Vapor Interfaces: A Computer Simulation Study. *J. Am. Chem. Soc.* **2006**, *128* (43), 14166–14175, DOI 10.1021/ja061901w.
- (40) Jorgensen, W. L.; Maxwell, D. S.; Tirado-Rives, J. Development and Testing of the OPLS All-Atom Force Field on Conformational Energetics and Properties of Organic Liquids. *J. Am. Chem. Soc.* **1996**, *118* (45), 11225–11236, DOI 10.1021/ja9621760.
- (41) Berendsen, H. J. C.; Grigera, J. R.; Straatsma, T. P. The Missing Term in Effective Pair Potentials. *J. Phys. Chem.* **1987**, *91* (24), 6269–6271, DOI 10.1021/j100308a038.
- (42) Humphrey, W.; Dalke, A.; Schulten, K. VMD: Visual Molecular Dynamics. *J. Mol. Graph.*1996, 14 (October 1995), 33–38, DOI 10.1016/0263-7855(96)00018-5.
- (43) Dahal, U. R.; Dormidontova, E. E. The Dynamics of Solvation Dictates the Conformation of Polyethylene Oxide in Aqueous, Isobutyric Acid and Binary Solutions. *Phys. Chem. Chem. Phys.* **2017**, *19* (15), 9823–9832, DOI 10.1039/c7cp00526a.
- (44) Milner, S. T.; Witten, T. A.; Cates, M. E. Theory of the Grafted Polymer Brush. *Macromolecules* **1988**, *21* (8), 2610–2619, DOI 10.1021/ma00186a051.